Seasonal influenza circulation patterns and projections for September 2025 to September 2026

John Huddleston[1]**, Jennifer Chang**[1]**, Jover Lee**[1]**, Philippa Steinberg**[1]**, Richard A. Neher**[2] **& Trevor Bedford**[1,3]

[1]Vaccine and Infectious Disease Division, Fred Hutchinson Cancer Center, Seattle, WA, USA, [2]Biozentrum, University of Basel, Basel, Switzerland, [3]Howard Hughes Medical Institute, Seattle, WA, USA

September 23, 2025

Abstract

This report details current seasonal influenza circulation patterns as of mid-September 2025 and was prepared for the VCM ahead of the South Hemisphere VCM on September 19, 2025. This is not meant as a comprehensive report, but is instead intended as particular observations that we've made that may be of relevance. Please also note that observed patterns reflect the GISAID database and may not be entirely representative of underlying dynamics. All analyses are based on the Nextstrain pipeline [1, 2] with continual updates posted to nextstrain.org/seasonal-flu. *In compliance with data sharing agreements, this public version of the report does not include raw serological measurements.* **A/H1N1pdm:** D.3 continues to sweep globally likely due to reassortment with different NA backgrounds. We define the new HA clade D.3.1 to track this reassortant group. This clade continues to diversify genetically with at least one major subclade rising to high frequency in Europe, carrying 113K, 139D, and 283K substitutions. A/Wisconsin/67/2022 effectively covers recent viruses except those carrying HA1:155E or 155R substitutions. Our prediction models suggest that vaccine candidates in the D.3.1 subclade bearing 113K represent the closest antigenic match to the future population. **A/H3N2:** J.2.4 (with HA1 189R and 135K) is growing rapidly in Africa, Europe, North America, and Oceania, shows strong antigenic drift in ferrets, and is predicted to fix in these regions. J.2 with 145N and 261Q is growing rapidly in Southeast Asia and shows strong antigenic drift in humans. J.2.4, J.2.3 (189R and 158K), and J.2.5 (145N and 158K) are poorly covered by A/DistrictOfColumbia/27/2023 and A/Croatia/10136RV/2023. We predict J.2.4 vaccine candidates like A/Sydney/1359/2024, A/Nepal/N042/2025-egg, and A/Singapore/GP20238/2024-egg are best matched to the future population, although sera to these strains poorly cover other circulating viruses. **B/Vic:** The subclade C.3.1 is growing in North America with a strong signal of antigenic drift from ferret HI data associated with an HA1 197N substitution. The newly defined subclade C.3.1 shows evidence of reassortment to the NA background of HA subclade C.5.1. C.5.7 and C.5.1 appear to be declining globally as C.5.6.1 grows. Sera against B/Pennsylvania/14/2025 appears to cover C.3.1 and other extant clades.

Contents

Methods and Notes

Sequence data and subsampling

We base our analysis on sequence data available in GISAID as of September 18, 2025 and titer data available as of September 18. The availability of sequences varies greatly across time and geography and we try to minimize geographical and temporal bias by subsampling the data or analyzing different geographical regions separately when appropriate. While this subsampling reduces geographical biases, it doesn't remove this bias entirely.

Phylogenetic analysis

The database contains too many sequences to perform a comprehensive phylogenetic analysis of all available data. We hence subsample the data to at least 3000 sequences collected in the last 2 years. To minimize bias from differences in surveillance intensity, we evenly sample at most 2700 sequences (90%) across region, year and month bins for regions including North America, Oceania, China, South America, West Asia, Japan and Korea, Southeast Asia, Africa, and South Asia. For European data, we sample at most 300 sequences (10%) across country, year and month bins. Within each region/country, year, and month group, we prioritize sequences with corresponding antigenic data. For phylogenetic context, we include an additional 300 sequences collected prior to 2 years ago and as early as January 2016, evenly sampling by region and year. We also include all strains with titer measurements as a test or reference virus, to ensure that all titer data are available to observe in our interactive reports.

Parallel evolution, that is repeated occurrence of identical substitutions in different clades of the tree, is common in A/H3N2 and A/H1N1pdm. Such parallel evolution violates fundamental assumptions of common phylogeny software and can erroneously group distinct clades together if they share too many parallel changes. To avoid such artifacts, we mask sites with rampant parallelism prior to phylogeny inference.

Clades and subclades are assigned using a collection of "signature" mutations available at the GitHub repository github.com/nextstrain/seasonal-flu for each lineage via the following links:

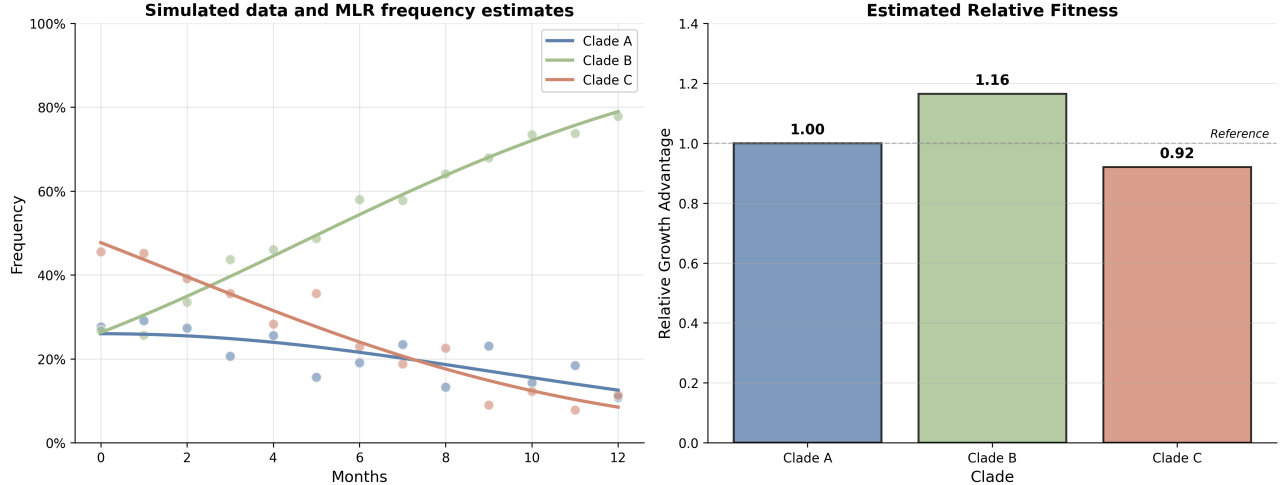- H1N1pdm HA
- H1N1pdm NA
- H3N2 HA
- H3N2 NA
- Vic HA
- Vic NA

Frequency and fitness estimates

Although phylogenetic analyses require a subset of all available sequences to produce an unbiased tree, we apply a non-phylogenetic method to estimate clade frequencies from all hemagglutinin (HA) sequences per lineage. We align all HA sequences to the lineage's reference sequence using Nextclade and obtain clade labels and amino acid substitutions per sequence [3]. From these Nextclade annotations per sequence, we jointly estimate the frequencies and relative growth advantages of each clade per geographic region in 14-day intervals using a hierarchical multinomial logistic regression

(MLR) model [4]. Multinomial logistic regression across n variants models the probability of a virus sampled at time t belonging to variant i as equal to its frequency $x_i(t)$ following

$$\Pr(X = i) = x_i(t) = \frac{p_i \exp(f_i\, t)}{\sum_j p_j \exp(f_j\, t)}.$$

A toy example of MLR fit to frequency data is shown in Figure 1.

Figure 1. Demo of MLR model and directly estimating clade-level growth advantage from frequency dynamics.

Growth advantages reflect the advantage of each clade relative to a specific reference clade or "pivot" clade. Values less than 1 indicate lower fitness than the pivot clade and values greater than 1 indicate higher fitness. In addition to estimating region-specific growth advantages, the model estimates an average growth advantage and variance per clade across all regions which we report as the "hierarchical GA". The hierarchical GA is analogous to the local branching index in that it reflects the recent global success of each clade. The region-specific GA is analogous to a region-specific local branching index.
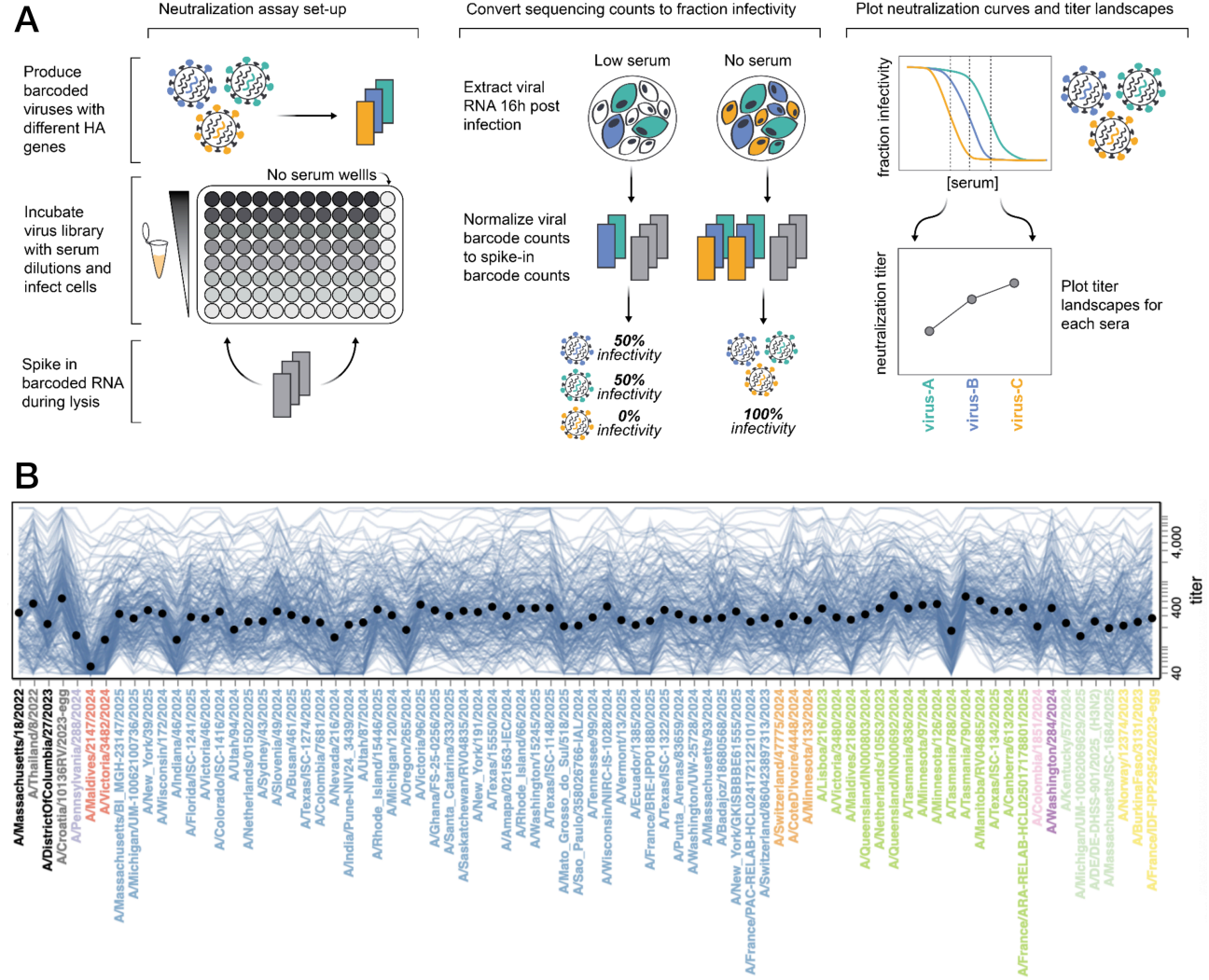
Antigenic analysis of ferret data

We summarize HI and FRA measurements provided by the WHO CCs in London, Melbourne, Atlanta, and Tokyo using our *substitution model* [5] which models log-titers as a sum of effects associated with amino acid differences between the sequences of the test and reference virus. In addition, the model allows for a serum (column) and a virus (row) effect. This model allows inference of titers for virus/serum pairs that have not been antigenically characterized and isolates effects consistently observed across many measurements from the noise inherent in individual measurements. We also plot individual and average normalized $\log_2$ titers per reference serum for test viruses in specific clades, to represent the raw antigenic data available for each influenza lineage.

In addition to the MLR-based growth advantages described above, we estimated the fitness of currently circulating strains using antigenic advance based on titer measurements from ferret sera [5]. High antigenic advance indicates groups of viruses with amino acid substitutions that are inferred to increase the antigenic distance from viruses without those substitutions.

4

High throughput human serology and antigenic analysis

Kikawa et al. [6] describes the generation of a library of 76 recently circulating H3N2 strains and 38 recently circulating human H1N1pdm strains, as well as 26 historical vaccine strains for H3N2 and H1N1pdm (Fig. 2A). This work uses a high-throughput sequencing-based neutralization assay to measure neutralization titers for these 140 viruses against a panel of 188 human sera collected from individuals spanning from young children to elderly adults, drawn from four sites around the world and collected between October 2024 and April 2025. Variation in titer is clear across individuals and across viruses (Fig. 2B). We apply the same 'titer model' as used for ferret data [5] to predict antigenic escape for strains that were not directly measured in the assay. In this report we focus on a subset of test viruses which are cell-passaged (N=39 H1N1pdm and N=77 H3N2) and the subset of human sera that were not known to be post-vaccination (N=181).

Figure 2. High-throughput sequencing-based neutralization to measure human serological responses across viruses. (A) Sequencing-based neutralization assays enable rapid measurement of titers against many strains. (B) Titers of individual human sera to recent H3N2 strains. Figure reproduced from Kikawa et al. [6].

Antigenic distance to the predicted future population

To rank vaccine candidates per subtype by their antigenic distance to the future, we integrated antigenic distance estimated from human or ferret serological data with predicted future frequencies estimated by the MLR model. The MLR model allows us to predict future frequencies of emerging haplotypes per geographic region. Our titer substitution model [5] estimates the antigenic effect of each HA1 substitution between reference and test viruses. For each reference virus used in ferret cell HI experiments (vaccine candidates), we calculated the average antigenic distance between that candidate's HA1 amino acid sequence and the corresponding HA1 sequence for each virus in each combination of emerging haplotype and geographic region. We calculated each pairwise antigenic distance between the candidate and another virus sequence as the sum of antigenic effects associated with the substitutions between the two viral HA1 sequences. We calculated a weighted average antigenic distance to the future by multiplying the predicted future frequency of each haplotype in a given region (e.g., Fig. 4) by the average antigenic distance for that haplotype/region combination. Finally, we averaged these estimates across regions to get the weighted average antigenic distance for the vaccine strain to the predicted future population. Candidates with the lowest distances are predicted to be the best representatives of the future population.
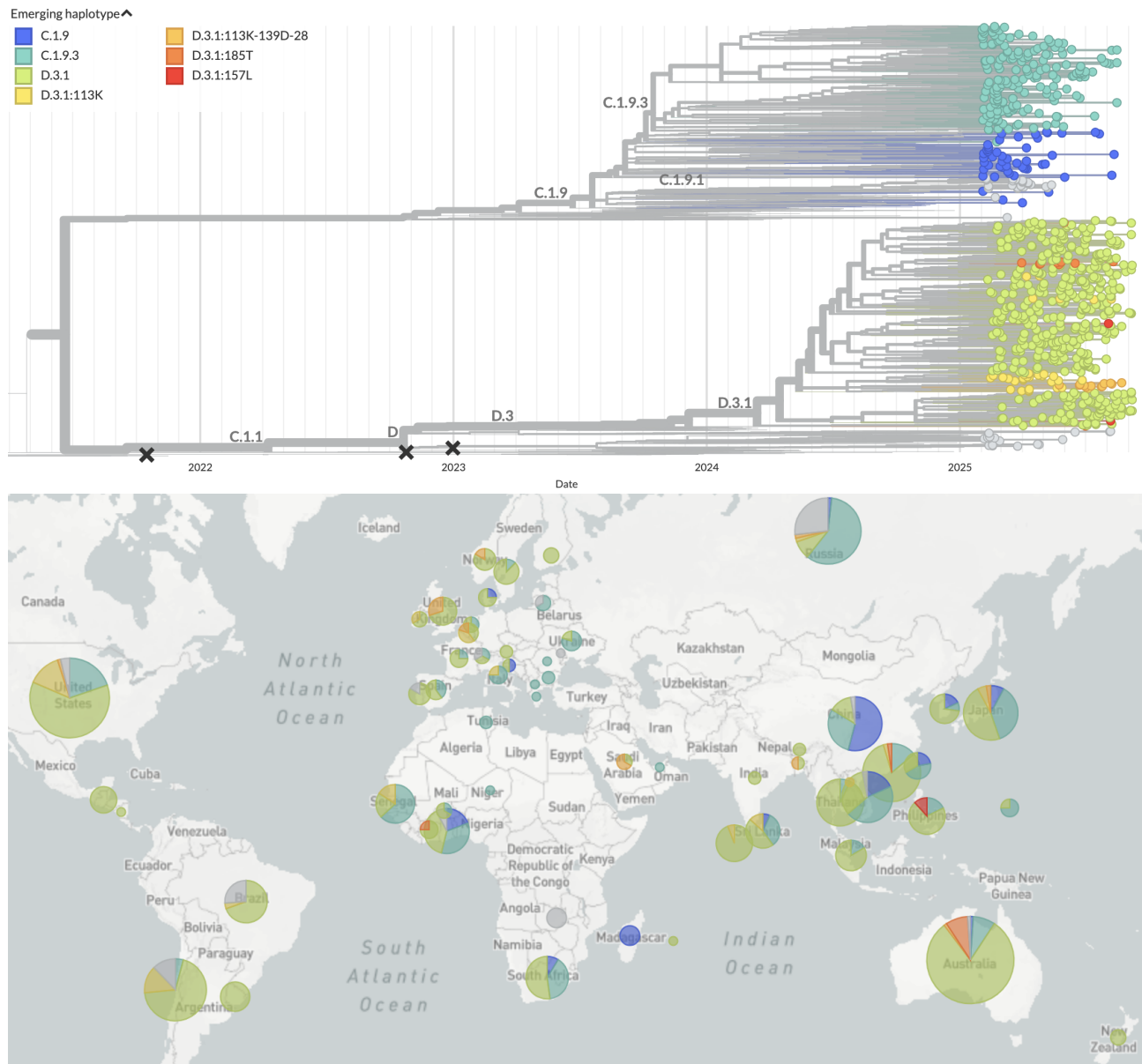
A/H1N1pdm

D.3 continues to sweep globally likely due to reassortment with different NA backgrounds. We define the new HA clade D.3.1 to track this reassortant group. This clade continues to diversify genetically with at least one major subclade rising to high frequency in Europe, carrying 113K, 139D, and 283K substitutions. A/Wisconsin/67/2022 effectively covers recent viruses except those carrying HA1:155E or 155R substitutions. Our prediction models suggest that vaccine candidates in the D.3.1 subclade bearing 113K represent the closest antigenic match to the future population.
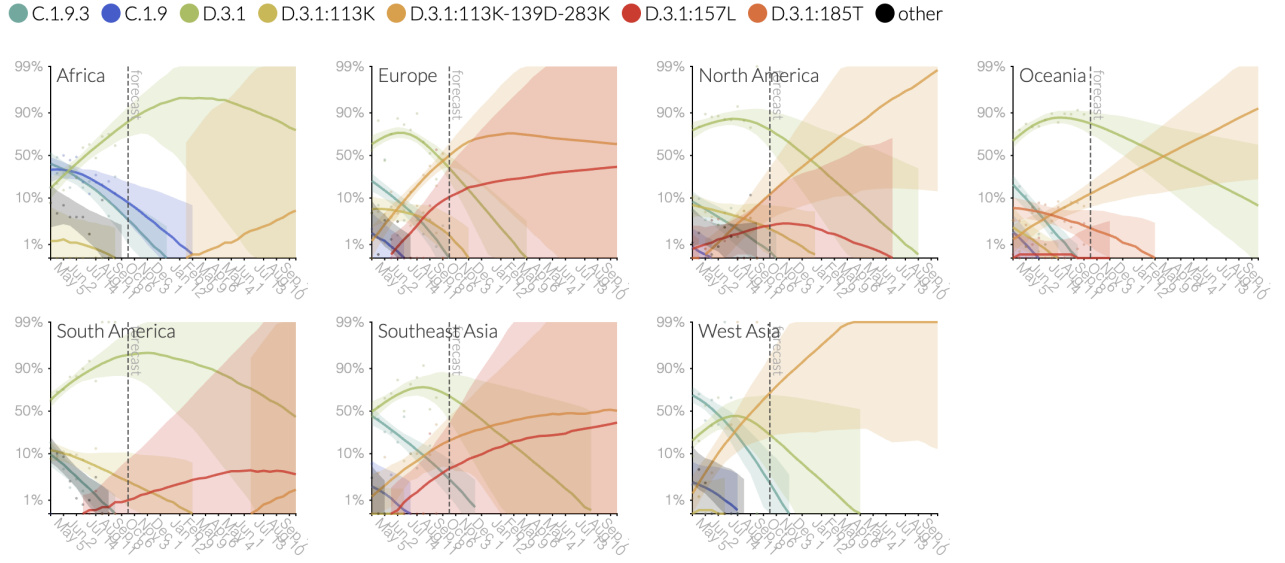
Current circulation patterns

In the six months since the last VCM, D.3 has swept to fixation in every region except Africa, China, and Southeast Asia where it is growing rapidly (Figs. 3 and 4). The recently successful subclade D.3.1 lacks HA1 substitutions relative to D.3 that could explain its success, but this clade has reassorted with multiple NA backgrounds including the NA subclade D.1 (formerly C.5.3.1 with A98V substitution). These reassortment events may explain D.3.1's consistently higher growth advantage over all other clades across all regions (Fig. 5).

Now that D.3 has essentially fixed, we note three emerging haplotypes including D.3.1:113K, D.3.1:113K-139D-293K, and D.3.1:185T. D.3.1:113K has reassorted with two different NA backgrounds including a small subclade with NA:V263I and the larger NA subclade D.2 (D with NA:52N). This clade never reached high frequency globally this year and continues to have a lower growth advantage across all regions (Fig. 5). In contrast, D.3.1:113K-139D-293K has circulated in five regions including Southeast Asia, has reassorted with an NA subclade D with a M314I substitution, and has the highest growth advantage across all regions (Fig. 5). A subclade of D.3.1:113K-139D-293K carries an additional HA1:K302E substitution that is associated primarily with recent European sequences. D.3.1:185T has only been collected in Australia and New Zealand and circulates with an NA subclade D.1 with A81V. Given its limited geographic distribution, we can only say that D.3.1:185T's growth advantage is similar to D.3.1 in Oceania. The HA1 sites 139 and 185 are both putative epitope sites.
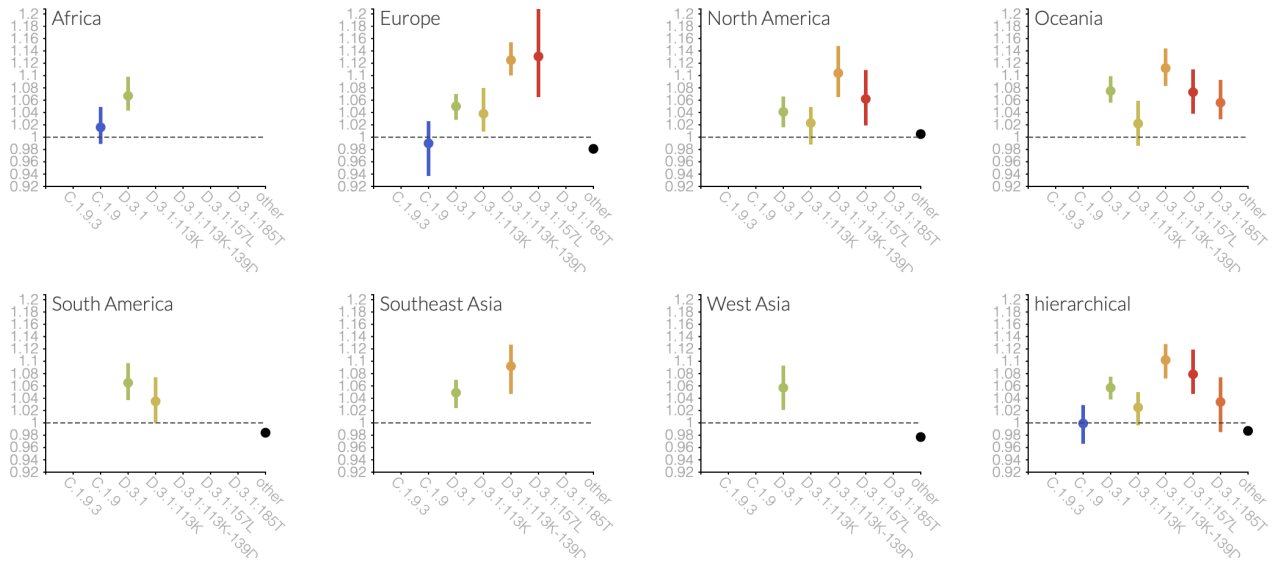
A subset of recent D.3.1 viruses have acquired a HA1:157L substitution. These viruses have been collected primarily in Denmark (N=67) with fewer than 5 samples collected in the USA, Australia, Thailand, or the Philippines. As a result of the recent samples from Denmark, we estimate a high growth advantage for D.3.1:157L viruses (Fig. 5). We also observe modest antigenic advance for these viruses from titer models fit to serological data from both ferrets (Fig. 6) and humans (Fig. 7). Given the global rarity of this substitution at the moment, we do not have enough evidence to be sure of its fitness compared to other haplotypes.

Figure 3. Time-resolved A/H1N1pdm phylogeny colored by clade and filtered to strains collected since February 1, 2025 (top) and corresponding geographic distribution of strains shown in the phylogeny (bottom). View on nextstrain.org.

Figure 4. Clade frequencies by region estimated by a multinomial logistic regression (MLR) model. Lines show the median frequency estimated under an assumption of exponential growth. Shading indicates 95% lower and upper highest posterior density intervals from the model. Colored points indicate frequency estimates from the raw data binned into biweekly intervals. Selection manifests as straight lines on the logit scale of the y-axis where the slope corresponds to the strength of selection per clade. Forecasts show MLR model predictions at biweekly steps up to 1 year in the future. View on Nextstrain.

Figure 5. Growth advantages per clade by region as estimated by a MLR model. The "hierarchical" advantage represents the global average fitness per clade. The dashed vertical line at x=1 indicates the growth advantage of the pivot clade. Clades with growth advantages greater than 1 have a higher fitness than the pivot. Colored points indicate the median growth advantage per clade and location. Error bars indicate the 95% lower and upper highest posterior density intervals from the model. View on Nextstrain.

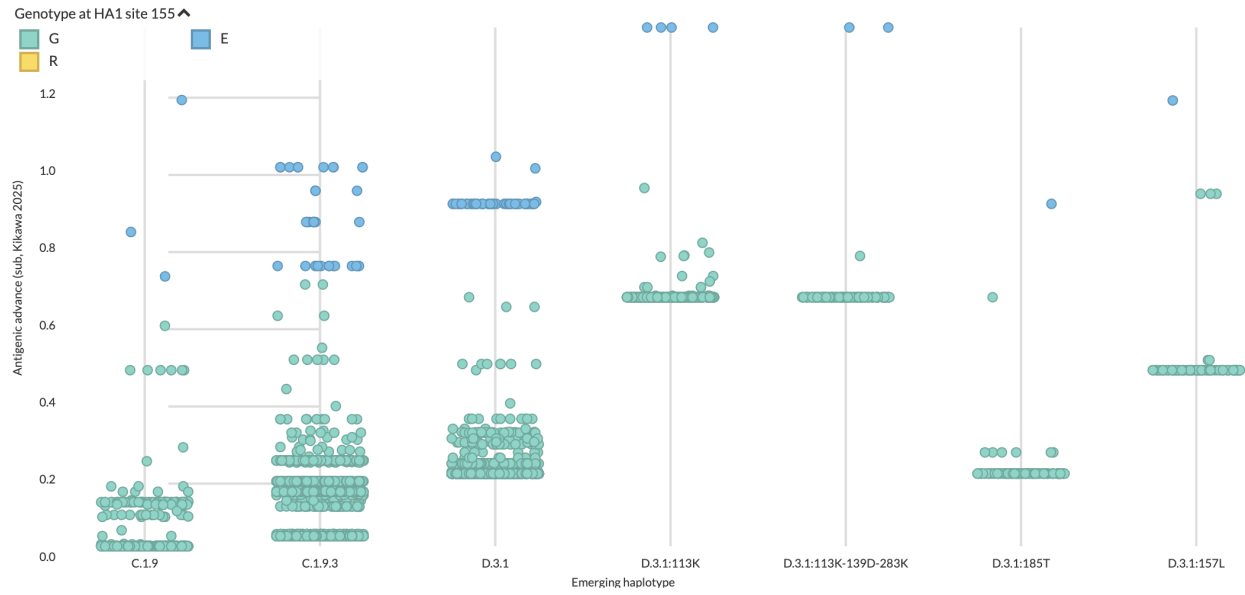## Antigenic properties from ferret and individual human serology

[Raw ferret data redacted]

From the ferret data, we see only a weak signal of antigenic advance for most test viruses in D.3.1 that does not fully explain that clade's recent rapid growth globally (Fig. 6). A subset of test viruses carrying HA1 substitutions of G155R or G155E show 1-2 $\log_2$ units increase in antigenic advance relative to the ancestral D.3.1 viruses.

Figure 6. Antigenic advancement across clades estimated from ferret-based HI data [5] for samples collected since February 1, 2025.
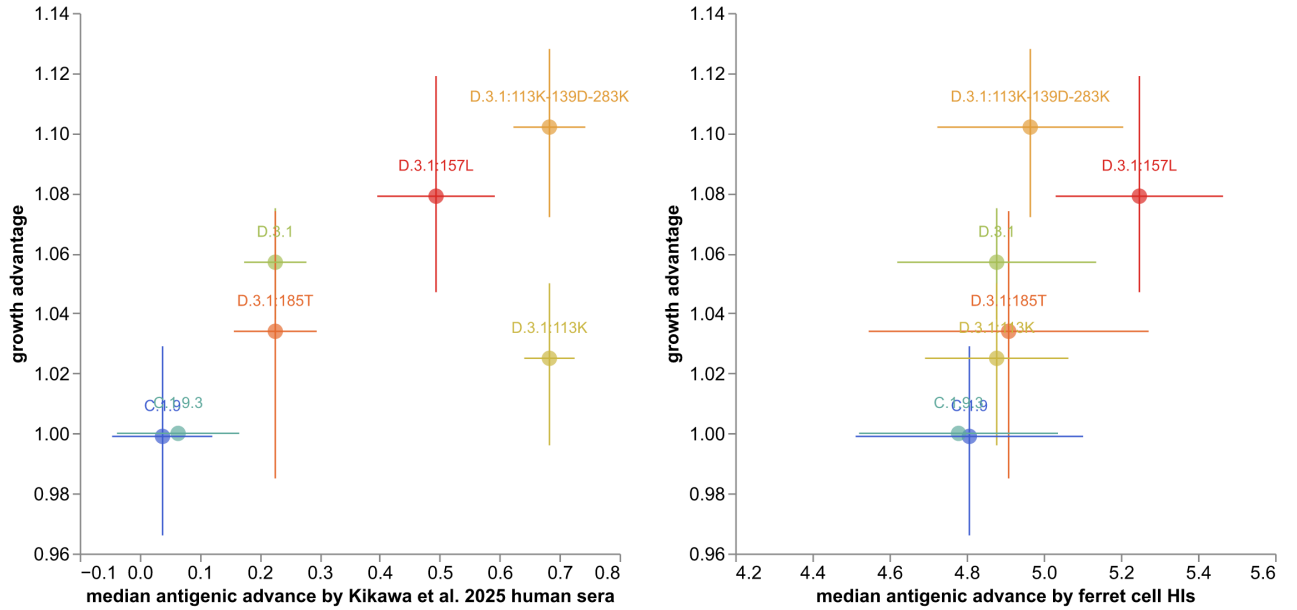
We also fit titer models to neutralization titers for recently collected human sera and H1N1pdm viruses as detailed in Kikawa et al. [6]. Unlike the ferret data, we see modest antigenic advancement in D.3.1 and greater advancement for D.3.1 viruses bearing HA1:113K (Fig. 7). These neutralization data did not include test viruses from the recent D.3.1:113K-139D-283K group, so we cannot ascertain if this group is more advanced than D.3.1:113K on its own. However, as in the ferret data, we observe a strong antigenic effect for HA1 155E substitutions in these human data.

Figure 7. Antigenic advancement across clades estimated with a titer substitution model [5] from human-based neutralization data [6].

Comparing viral fitness forecasts and antigenic phenotype
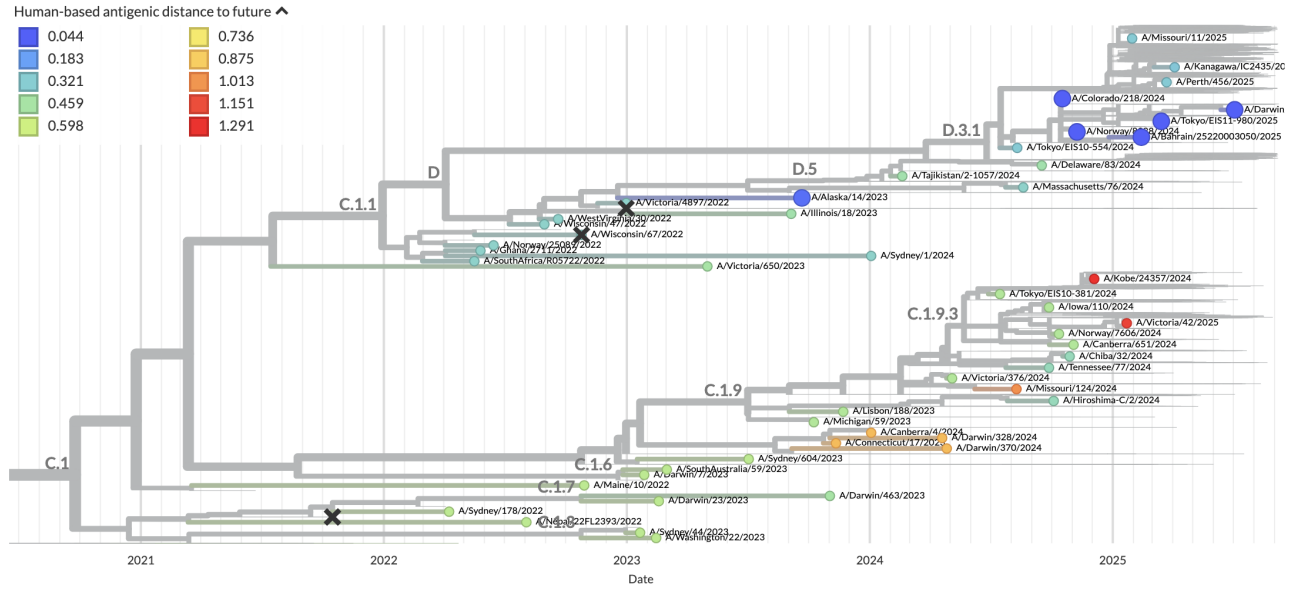
To understand the relationship between viral fitness estimated from frequency dynamics (growth advantages from the MLR model) vs from experimental data (antigenic advancement), we plotted the growth advantage of each recent emerging haplotype against the corresponding median antigenic advance of sequences in that haplotype based on human or ferret serological data. With both ferret and human measurements of antigenic phenotype, we find that growth advantages from frequency behavior correspond well to antigenic advancement (Fig. 8). The D.3.1:113K haplotype is one exception where human antigenic advance suggests this haplotype should be more successful than it is. The human antigenic advance clearly distinguish C.1.9.3, D.3.1, and D.3.1:113K haplotypes. 139D and 283K were not present in the libaries from Kikawa et al. [6] and so the lack of difference in antigenic advancement between D.3.1:113K and D.3.1:113K-139D-283K is potentially an artifact of experimental setup. In contrast, the ferret advance values overlap substantially for all of these haplotypes.
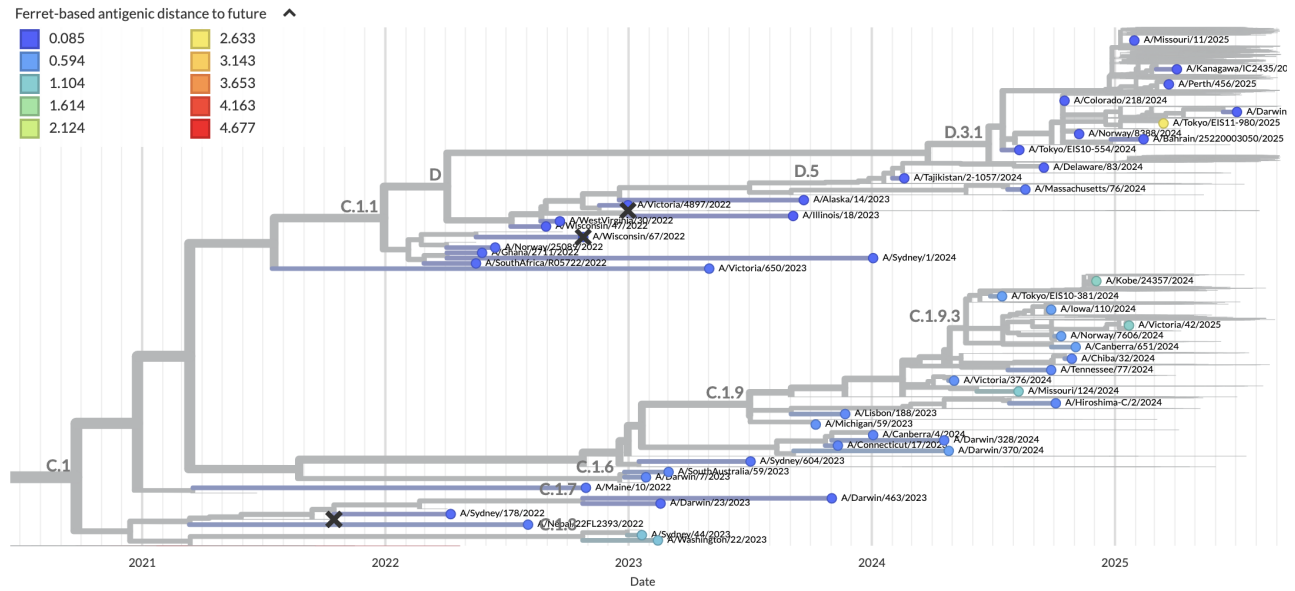

Figure 8. Growth advantage by antigenic advance per clade estimated with a titer substitution model [5] for human-based neutralization data [6] (left) and ferret-based cell HI data (right). Growth advantages shown as median +/- 95% HPDIs. Antigenic advance shown as median +/- 1 standard deviation across all sequences in a given clade.

Finally, we ranked the available vaccine candidates by their antigenic distance to the predicted future H1N1pdm population as described in the Methods. We found that viruses from D.3.1:113K like A/Colorado/218/2024 or A/Norway/8388/2024 were closest to the predicted future, followed by other viruses in D.3.1 (Fig. 9). We also noted that the current vaccine strain, A/Wisconsin/67/2022, is similarly close to the predicted future as other D.3.1 candidates outside of the 113K group. We found that A/Alaska/14/2023 was predicted to be close to the future population, most likely reflecting that A/Alaska/14/2023 also has a HA1 113K substitution. However, we only have one ferret cell HI measurement between that reference strain and recent D.3.1 viruses to know whether it would effectively cover D.3.1 viruses. In contrast to these distances based on human antigenic advance, distances based on ferret antigenic advance did not distinguish between viruses descending from C.1.1 (Fig. 10).

Figure 9. Weighted average antigenic distance to the future population per reference virus using human-based neutralization data. For each reference virus, we calculated the average antigenic distance between that virus's HA1 amino acid sequence and the corresponding HA1 sequences for viruses from each emerging haplotype and geographic region. The pairwise antigenic distance between viruses was based on the HA1 substitutions between them and antigenic weights per substitution estimated with a titer substitution model [5] fit to human-based neutralization data [6].
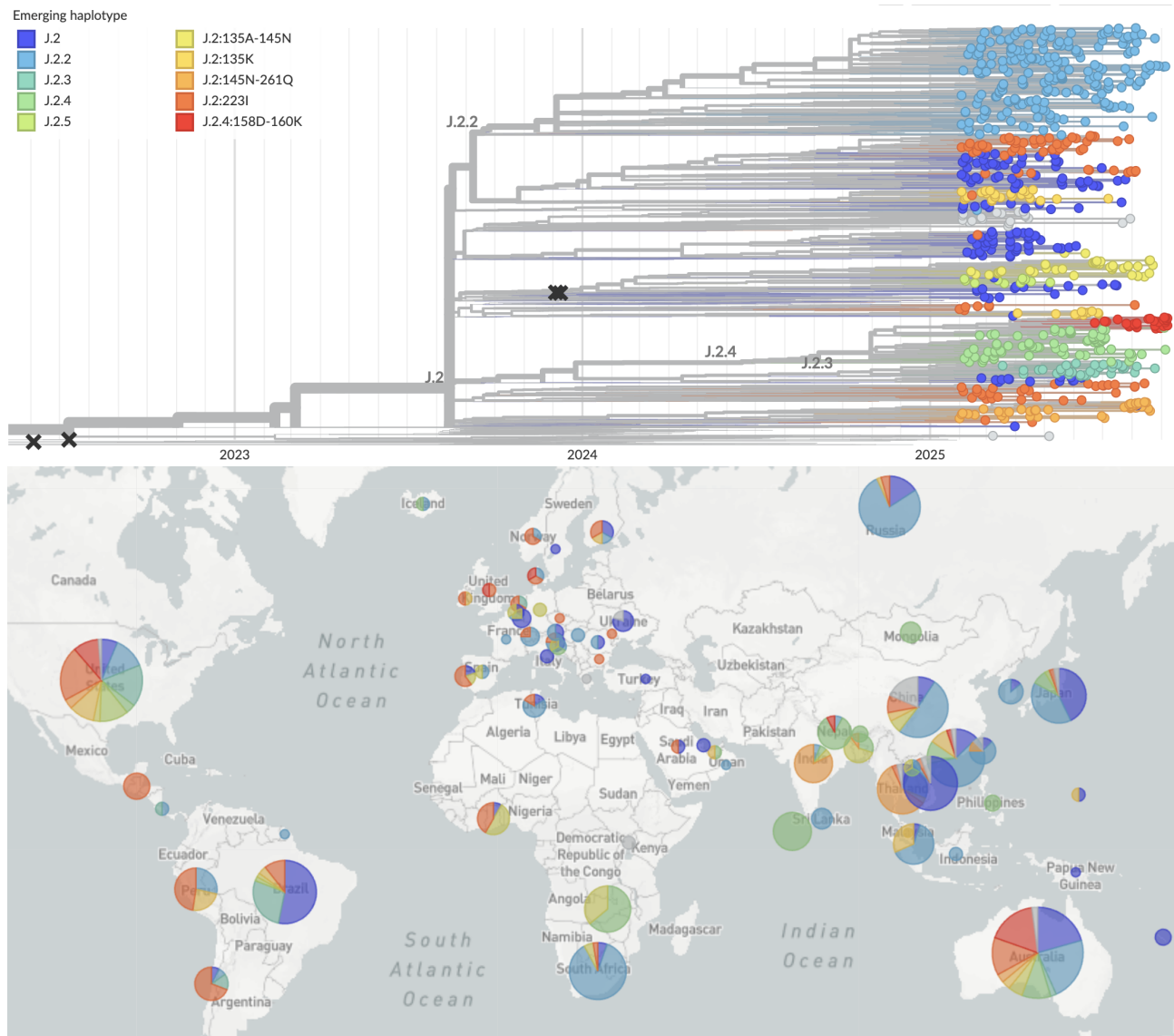

Figure 10. Weighted average antigenic distance to the future population per reference virus using ferret-based cell HI data. For each reference virus, we calculated the average antigenic distance between that virus's HA1 amino acid sequence and the corresponding HA1 sequences for viruses from each emerging haplotype and geographic region. The pairwise antigenic distance between viruses was based on the HA1 substitutions between them and antigenic weights per substitution estimated with a titer substitution model [5] fit to ferret-based cell HI data.
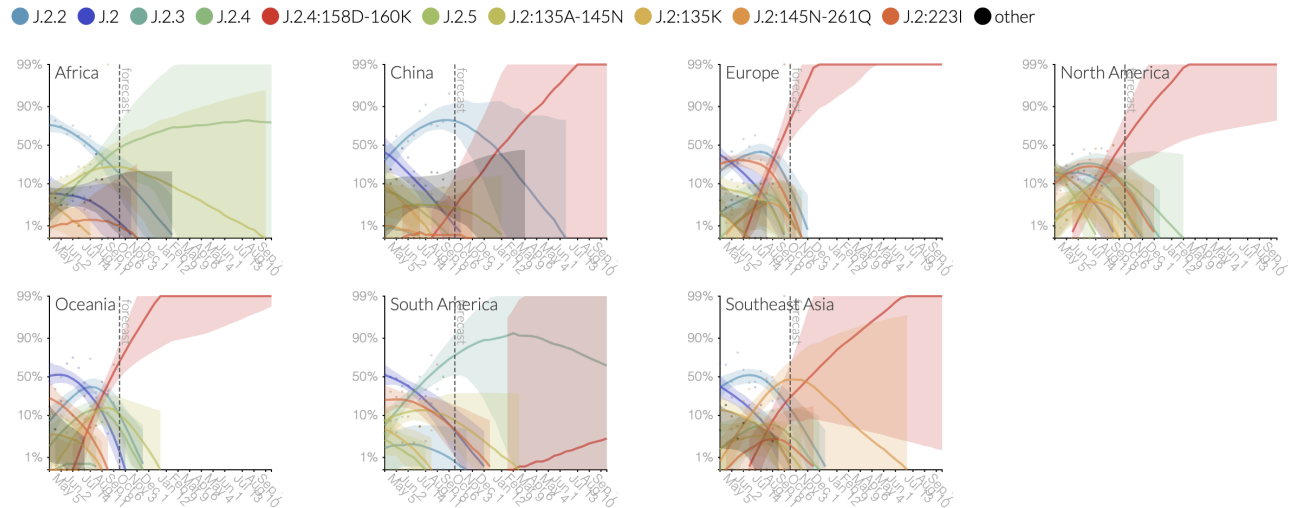
13

A/H3N2

J.2.4 (with HA1 189R and 135K) is growing rapidly in Africa, Europe, North America, and Oceania, shows strong antigenic drift in ferrets, and is predicted to fix in these regions. J.2 with 145N and 261Q is growing rapidly in Southeast Asia and shows strong antigenic drift in humans. J.2.4, J.2.3 (189R and 158K), and J.2.5 (145N and 158K) are poorly covered by A/DistrictOfColumbia/27/2023 and A/Croatia/10136RV/2023. We predict J.2.4 vaccine candidates like A/Sydney/1359/2024, A/Nepal/N042/2025-egg, and A/Singapore/GP20238/2024-egg are best matched to the future population, although sera to these strains poorly cover other circulating viruses.
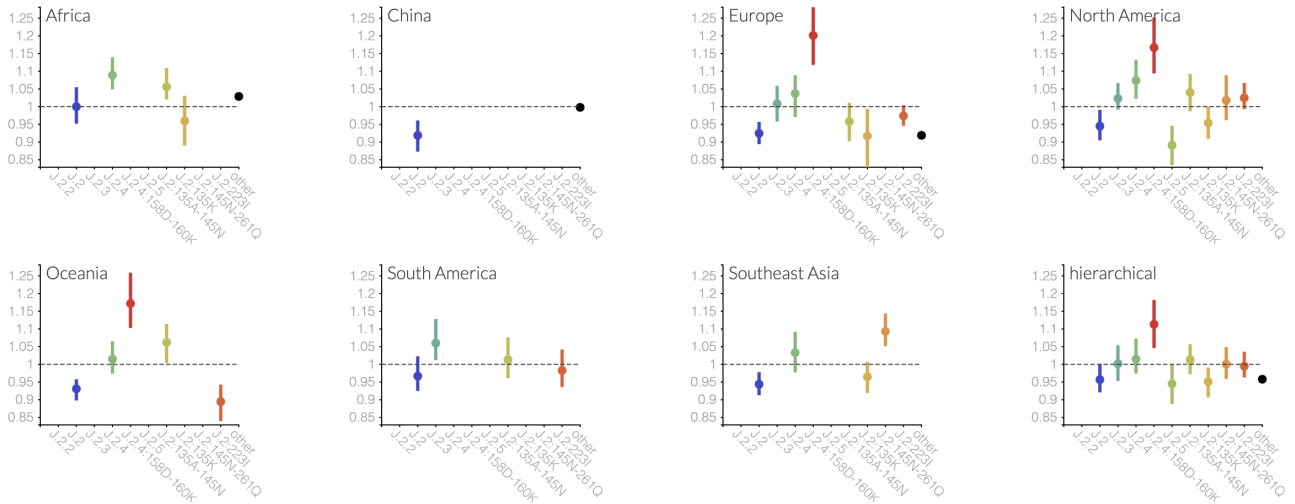
Current circulation patterns

J.2.4 (i.e. J.2 bearing HA1 mutations 135K and 189R) is growing rapidly in Africa, Europe, North America, and Oceania (Fig. 11). However, this growth is largely due to the presence of the a recent subclade of J.2.4 that carries additional HA1 substitutions including 158D, 160K, 328A, 144N, and 173R. This subclade is labeled as J.2.4:158D-160K and we predict this subclade will continue to expand over the coming year (Fig. 12). In the frequency projections J.2.4:158D-160K does not fix in Africa and South America only because it's not yet been sampled sufficiently in these regions, we believe it should spread widely. Another J.2 clade with HA1 145N and 261Q substitutions is also growing rapidly in Southeast Asia, although its fitness advantage is less clear than J.2.4's (Fig. 13). South America is the only region where J.2.3 appears to be growing at the expense of all other clades (Fig. 12). All other clades appear to be in decline across all regions.

Figure 11. Time-resolved A/H3N2 phylogeny colored by clade and filtered to strains collected since February 1, 2025 (top) and corresponding geographic distribution of strains shown in the phylogeny (bottom). View on nextstrain.org.

15

Figure 12. Clade frequencies by region estimated by multinomial logistic regression (MLR). Lines show the median frequency estimated under an assumption of exponential growth. Shading indicates 95% lower and upper highest posterior density intervals from the model. Colored points indicate frequency estimates from the raw data binned into biweekly intervals. Selection manifests as straight lines on the logit scale of the y-axis where a clade's slope corresponds to its strength of selection. Forecasts show MLR projections up to 1 year in the future. View on Nextstrain.

Figure 13. Growth advantages per clade by region as estimated by MLR. The "hierarchical" advantage represents the global average fitness per clade. The dashed vertical line at x=1 indicates the growth advantage of the pivot clade. Clades with growth advantages greater than 1 have a higher fitness than the pivot. Colored points indicate the median growth advantage per clade and location. Error bars indicate the 95% lower and upper highest posterior density intervals from the model. View on Nextstrain.
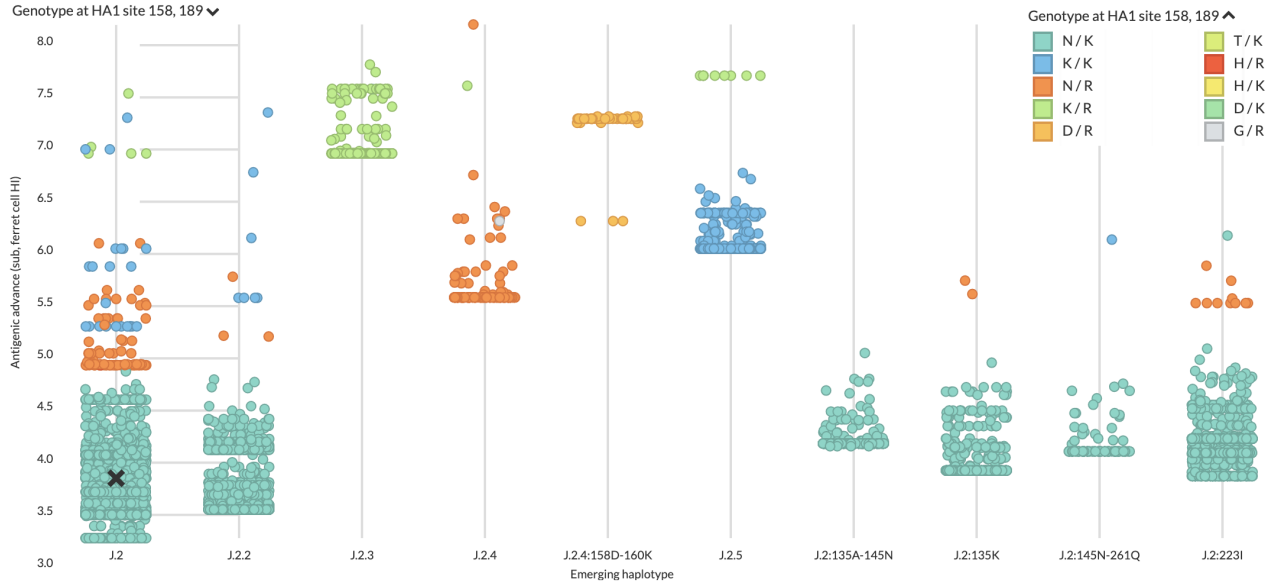
16

Antigenic properties from ferret and individual human serology
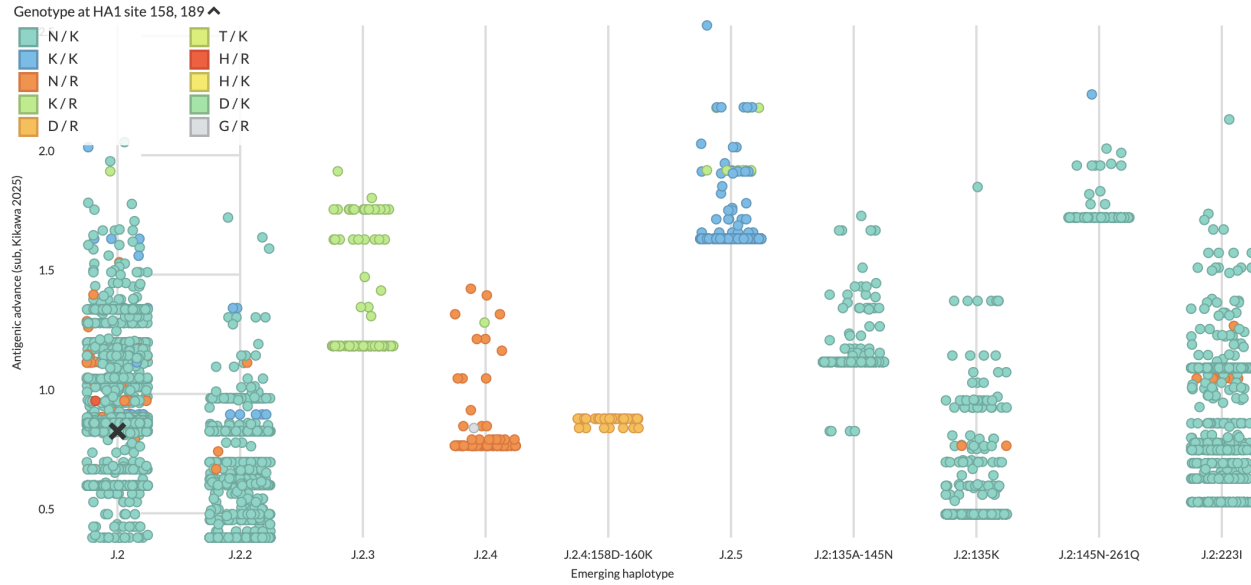
[Raw ferret data redacted]

When we calculated antigenic advance, aggregating ferret-based cell-passaged HI data from all collaborating centers, we found the highest advance associated with strains carrying 158K and 189R including subclades J.2.3, J.2.4, and J.2.5 (Fig. 14). Most viruses from the J.2.4:158D-160K subclade carry the following five HA1 substitutions with nonzero antigenic effects from the titer substitution model. These substitutions are listed below with their $\log_2$ effects:

- K158D:1.43
- I160K: 0.01
- T328A: 0.72
- S144N: 0.76
- Q173R: 0.22

We also fit titer models to neutralization titers for recently collected human sera and H3N2 viruses from Kikawa et al. [6]. Unlike the ferret data, human models show lower antigenic advance for J.2.4 corresponding to lower estimated effects of 135K and 189R (Fig. 15). The virus library for these neutralization experiments lacked viruses from J.2.4:158D-160K, so we cannot comment on the antigenic advance for the substitutions above from those data. The human models also show a slightly higher antigenic advance for J.2:145N-261Q viruses which could partially explain the recent success of these viruses in Southeast Asia.

Figure 14. Antigenic advance per clade estimated from ferret-based HI data [5] for samples collected since February 1, 2025. In each panel, points represent individual HA sequences whose overall antigenic advance has been inferred from a titer model based on the corresponding raw serological data.
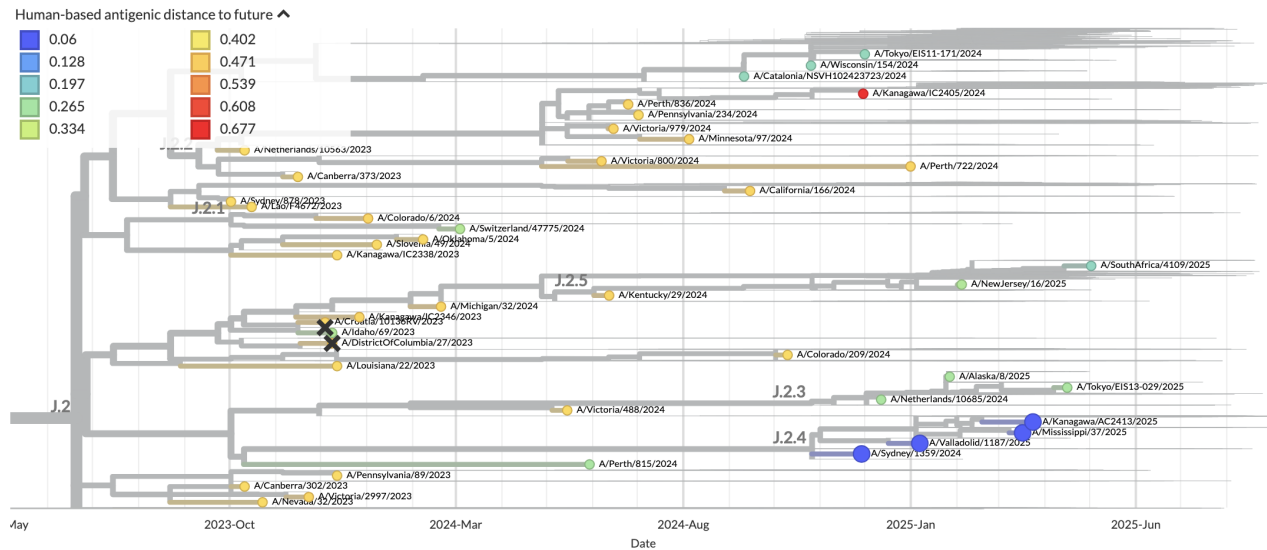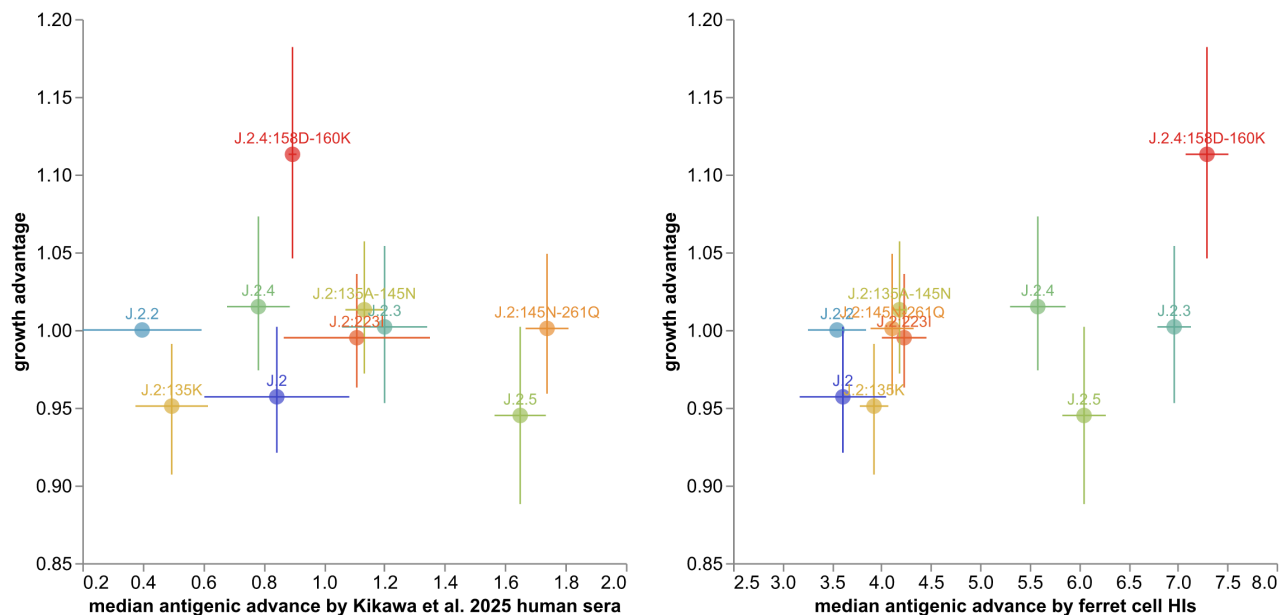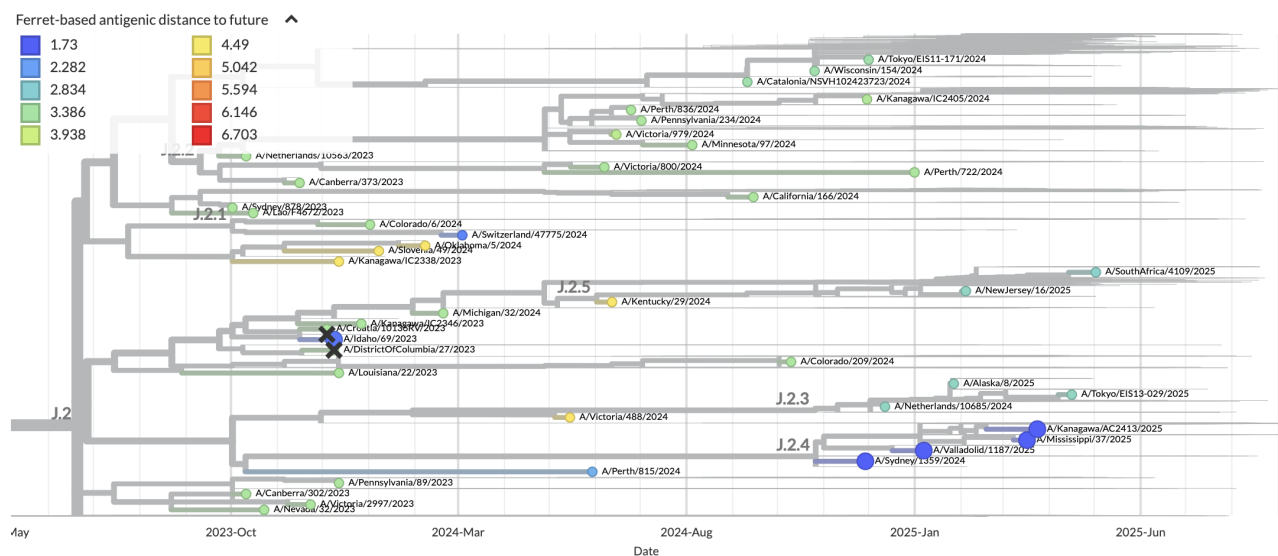
Figure 15. Antigenic advance per clade estimated with a titer substitution model [5] from human-based neutralization data [6].

Comparing viral fitness forecasts and antigenic phenotype

To understand the relationship between viral fitness estimated from sequence data alone (growth advantages from the MLR model) or from experimental data (antigenic advance), we plotted the growth advantage of each recent emerging haplotype against the corresponding median antigenic advance of sequences in that haplotype based on human or ferret serological data. With both measures of antigenic advance, we find that growth advantages from sequence data generally correspond well to antigenic advance (Fig. 16). J.2.5 has one of the highest antigenic advances by both species models, but it also has one of the lowest growth advantages. The human data / model finds higher antigenic advance for J.2:145N-261Q than the ferret model and fails to identify significant antigenic advancement for J.2.4 viruses despite their rapid growth. The ferret model identifies higher antigenic advance for both J.2.4 and J.2.4:158D-160K that correspond directly to the growth advantages we estimate for these haplotypes. However, the ferret model also identifies higher antigenic advance for J.2.3 than the human model despite the lack of growth for this clade.

Finally, we ranked the available vaccine candidates by their antigenic distance to the predicted future H3N2 population as described in the Methods. Results from both human and ferret antigenic models, found that J.2.4 reference viruses like A/Sydney/1359/2024 were closest to the predicted future (Figs. 17 and 18). Ferret-based antigenic distances also found that earlier J.2 viruses with the K189R substitution like A/Idaho/69/2023 were close to the future population. This result likely reflects the fact that ferret data detect higher antigenic advance for subclades with 189R like J.2.3 and J.2.4 than the human data detect.

Figure 16. Growth advantage by antigenic advance per clade estimated with a titer substitution model [5] for human-based neutralization data [6] (left) and ferret-based cell HI data (right). Growth advantages shown as median +/- 95% HPDIs. Antigenic advance shown as median +/- 1 standard deviation across all sequences in a given clade.

Figure 17. Weighted average antigenic distance to the future population per reference virus using human-based neutralization data. For each reference virus, we calculated the average antigenic distance between that virus's HA1 amino acid sequence and the corresponding HA1 sequences for viruses from each emerging haplotype and geographic region. The pairwise antigenic distance between viruses was based on the HA1 substitutions between them and antigenic weights per substitution estimated with a titer substitution model [5] fit to human-based neutralization data [6].

19

Figure 18. Weighted average antigenic distance to the future population per reference virus using ferret-based cell HI data. For each reference virus, we calculated the average antigenic distance between that virus's HA1 amino acid sequence and the corresponding HA1 sequences for viruses from each emerging haplotype and geographic region. The pairwise antigenic distance between viruses was based on the HA1 substitutions between them and antigenic weights per substitution estimated with a titer substitution model [5] fit to ferret-based cell HI data.

20

B/Vic

The subclade C.3.1 is growing in North America with a strong signal of antigenic drift from ferret HI data associated with an HA1 197N substitution. The newly defined subclade C.3.1 shows evidence of reassortment to the NA background of HA subclade C.5.1. C.5.7 and C.5.1 appear to be declining globally as C.5.6.1 grows. Sera against B/Pennsylvania/14/2025 appears to cover C.3.1 and other extant clades.
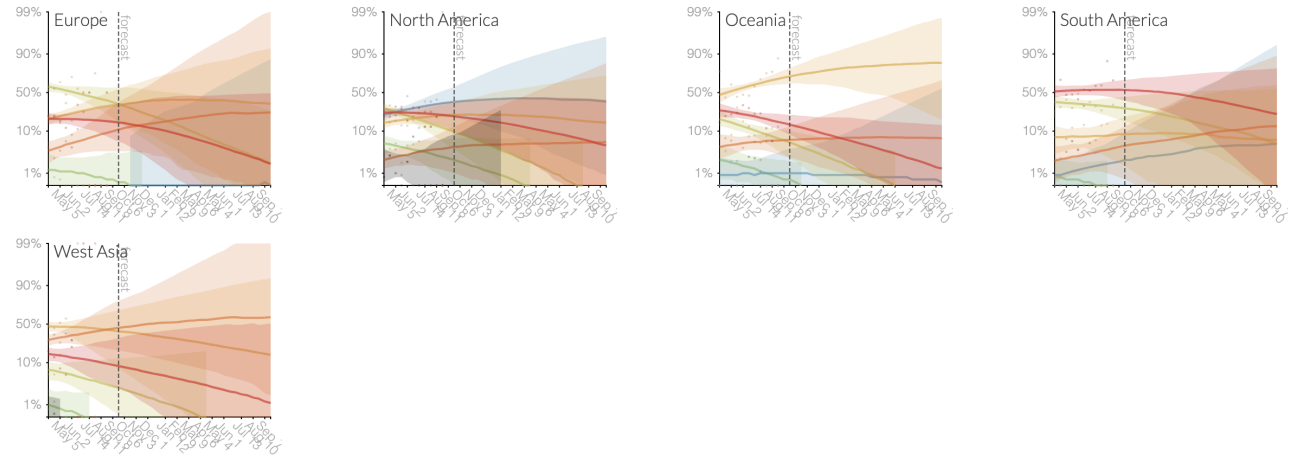
Current circulation patterns

Although clades C.5.1, C.5.6, and C.5.7 continue to cocirculate globally, clade C.3.1 has reemerged and grown in North America (Figs. 19 and 20). In this report, we define three new subclades to track variants with signals of antigenic drift from ferret serology:

- C.5.6.1 with HA1 37I, 128D, and 199A

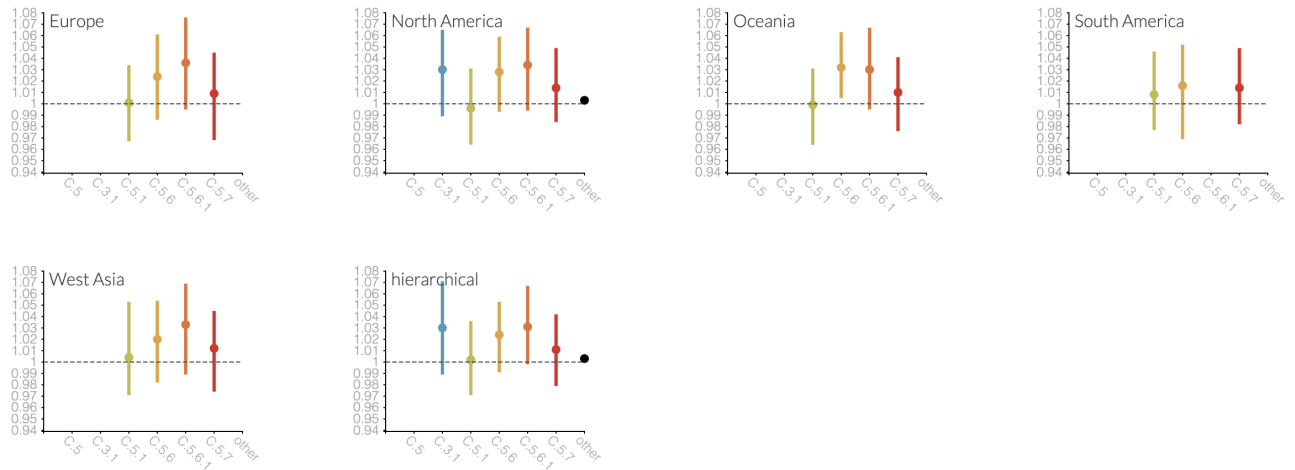- C.3.1 with HA1 197N and 208S

- C.3.2 with HA1 197N, 179H, and 208P

Most recent C.3 viruses descend from C.3.1 and appear to have reassorted from C.3's ancestral NA subclade of B.8 to C.5.1's NA subclade B.7.1. The recent growth of C.3 and C.3.1 contributes their high estimated fitnesses relative to the other three major clades (Fig. 21). C.3.1 does not appear to have spread widely outside of the USA.

Figure 19. Time-resolved B/Victoria phylogeny colored by clade and filtered to strains collected since February 1, 2025 (top) and corresponding country-level geographic distribution of strains shown in the phylogeny (bottom). View on nextstrain.org.

Figure 20. Clade frequencies by region estimated by a multinomial logistic regression (MLR) model. Lines show the median frequency estimated under an assumption of exponential growth. Shading indicates 95% lower and upper highest posterior density intervals from the model. Colored points indicate frequency estimates from the raw data binned into biweekly intervals. Selection manifests as straight lines on the logit scale of the y-axis where the slope corresponds to the strength of selection per clade. Forecasts show MLR model predictions at biweekly steps up to 1 year in the future. View on Nextstrain.

Figure 21. Growth advantages per clade by region as estimated by a MLR model. The "hierarchical" advantage represents the global average fitness per clade. The dashed vertical line at x=1 indicates the growth advantage of the pivot clade. Clades with growth advantages greater than 1 have a higher fitness than the pivot. Colored points indicate the median growth advantage per clade and location. Error bars indicate the 95% lower and upper highest posterior density intervals from the model. View on Nextstrain.

23

Antigenic properties from ferret and individual human serology

[Raw ferret data redacted]

Aggregating all cell-passaged HI data with a titer model, we find the highest antigenic advance is associated with recent C.3.1 strains (Fig. 22). We observe modest advance in C.5 subclades carrying HA1 T199A, P241K, and A202V. We observe the highest advance in C.5 subclades carrying HA1 L144P which has an estimated effect of 1.4 log2 units, but these viruses remain rare. We also fit a titer model to individual human HI titers from the VCM serology working group. This model shows that antigenic advance of C.3.1 was high due to its HA1 D197N substitution (Fig. 23). Variants within C.5.1, C.5.6, and C.5.7 had similar antigenic advances, too. Among those subclades, we observed recurrent antigenic effects for HA1 A154E (0.57 $\log_2$ units), D197N (0.51 $\log_2$ units), A202V (0.36 $\log_2$ units), and T199A (0.16 $\log_2$ units).

Figure 22. Antigenic advance per clade estimated from ferret-based HI data [5] for samples collected since February 1, 2025.
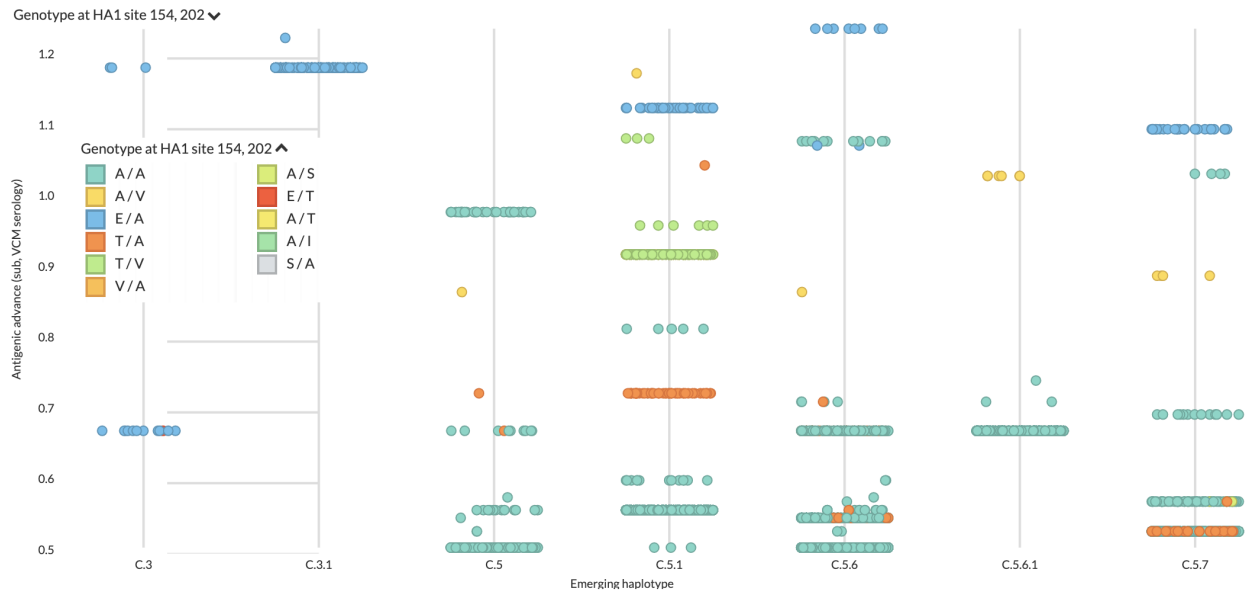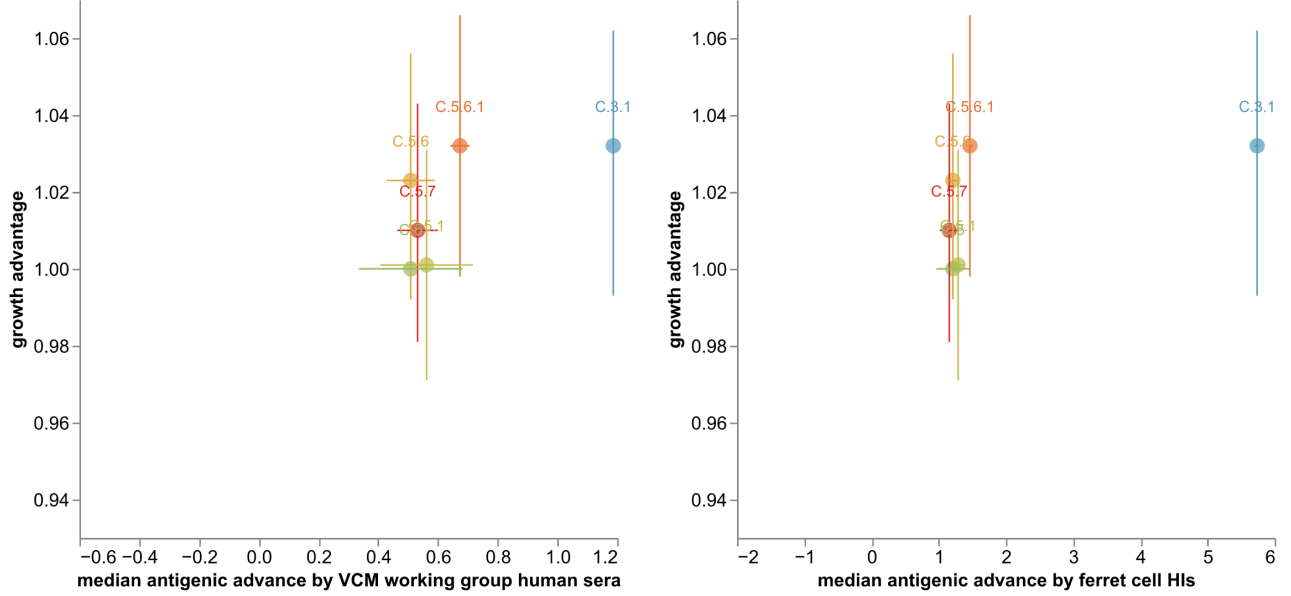
Figure 23. Antigenic advance per clade estimated with a titer substitution model [5] from human-based HI data from the VCM serology working group.
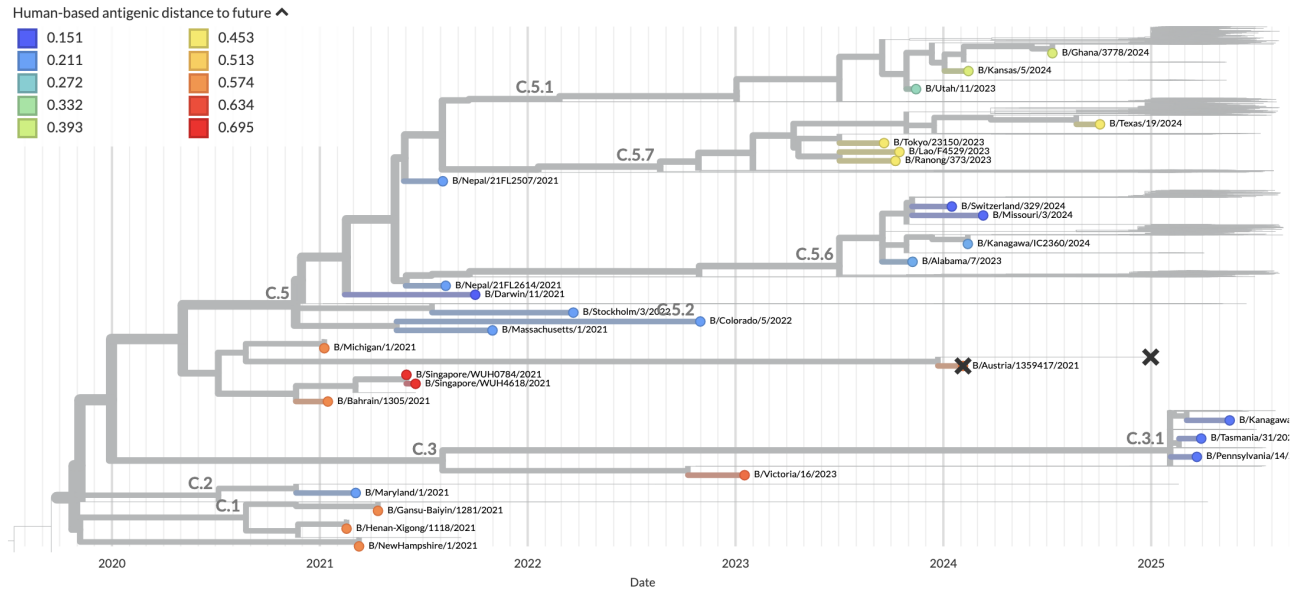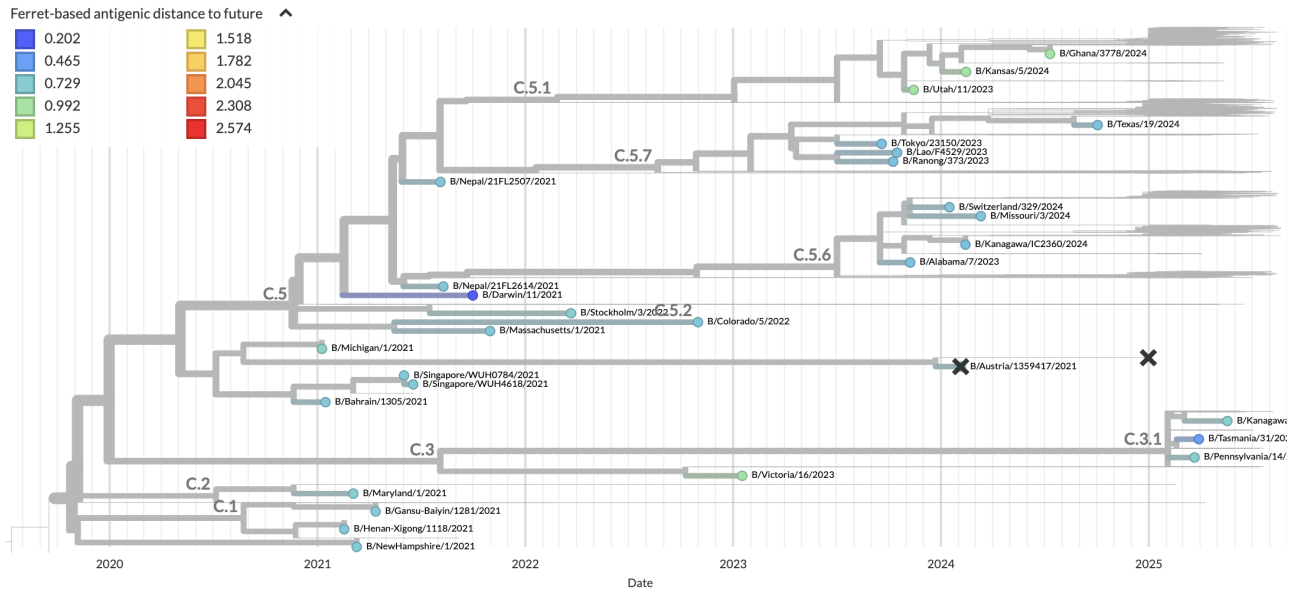
Comparing viral fitness forecasts and antigenic phenotype

As with our analysis H1N1pdm and H3N2 haplotypes, we find that growth advantages for Vic haplotypes correspond to antigenic advance estimated by human and ferret HI data (Fig. 24). However, this view highlights the degree to which ferret antigenic advance may be overestimating the immune escape of C.3.1 and potentially underestimating the potential immune escape of C.5.6.1.

Figure 24. Growth advantage by antigenic advance per clade estimated with a titer substitution model [5] for human-based HI data from the VCM serology working group (left) and ferret-based cell HI data (right). Growth advantages shown as median +/- 95% HPDIs. Antigenic advance shown as median +/- 1 standard deviation across all sequences in a given clade.

Finally, we ranked the available vaccine candidates by their antigenic distance to the predicted future Vic population as described in the Methods. Using the human antigenic model, we found that viruses from C.3.1 like B/Pennsylvania/14/2025, C.5.6 like B/Switzerland/329/2024 and B/Missouri/3/2024, and the C.5 reference B/Darwin/11/2021 were closest to the predicted future (Fig. 25). The close distance of C.3.1 references to the predicted future most likely reflects the fact that at least one of these viruses (B/Pennsylvania/14/2025) covers other circulating clades well, too. Using the ferret antigenic model, we found that B/Darwin/11/2021 was closest to the predicted future followed by B/Tasmania/31/2025 from C.3.1 (Fig. 26).

Figure 25. Weighted average antigenic distance to the future population per reference virus using human-based neutralization data. For each reference virus, we calculated the average antigenic distance between that virus's HA1 amino acid sequence and the corresponding HA1 sequences for viruses from each emerging haplotype and geographic region. The pairwise antigenic distance between viruses was based on the HA1 substitutions between them and antigenic weights per substitution estimated with a titer substitution model [5] fit to human-based neutralization data from the VCM serology working group.

Figure 26. Weighted average antigenic distance to the future population per reference virus using ferret-based cell HI data. For each reference virus, we calculated the average antigenic distance between that virus's HA1 amino acid sequence and the corresponding HA1 sequences for viruses from each emerging haplotype and geographic region. The pairwise antigenic distance between viruses was based on the HA1 substitutions between them and antigenic weights per substitution estimated with a titer substitution model [5] fit to ferret-based cell HI data.

Acknowledgments

References

1. Neher RA, Bedford T (2015) nextflu: real-time tracking of seasonal influenza virus evolution in humans. Bioinformatics 31: 3546–3548.

2. Hadfield J, Megill C, Bell SM, Huddleston J, Potter B, et al. (2018) Nextstrain: real-time tracking of pathogen evolution. Bioinformatics 34: 4121–4123.

3. Aksamentov I, Roemer C, Hodcroft EB, Neher RA (2021) Nextclade: clade assignment, mutation calling and quality control for viral genomes. Journal of Open Source Software 6: 3773.

4. Abousamra E, Figgins M, Bedford T (2024) Fitness models provide accurate short-term forecasts of SARS-CoV-2 variant frequency. PLoS Comput Biol 20: e1012443.

5. Neher RA, Bedford T, Daniels RS, Russell CA, Shraiman BI (2016) Prediction, dynamics, and visualization of antigenic phenotypes of seasonal influenza viruses. Proc Natl Acad Sci USA 113: E1701–E1709.

6. Kikawa C, Huddleston J, Loes AN, Turner SA, Lee J, et al. (2025) Near real-time data on the human neutralizing antibody landscape to influenza virus to inform vaccine-strain selection in September 2025. bioRxiv : 2025.09.06.674661.